Journal of Materials Chemistry C

ROYAL SOCIETY OF CHEMISTRY

PAPER

View Article Online
View Journal

Cite this: DOI: 10.1039/d5tc02868j

Photochromism and photofluorochromism of arylvinylene phenanthridines

Atul B. Nipate, Vinutha K. Venkatareddy and M. Rajeswara Rao*

Received 30th July 2025,
Accepted 26th November 2025

DOI: 10.1039/d5tc02868j

rsc.li/materials-c

Novel phenanthridine-based light-induced, multicolour photochromic π-conjugated compounds (**PC$_1$–PC$_3$**) have been developed. **PC$_1$–PC$_3$** were synthesised *via* Knoevenagel condensation on phenanthridine using various aromatic aldehydes [triphenylaminyl (TPA) and pyrenyl (PY)] in the presence of benzoic acid and benzoic anhydride in 63–70% yields. The compounds absorb strongly in the visible region (λ_{max} = 360–408 nm for **PC$_1$**, λ_{max} = 360 nm for **PC$_2$**, λ_{max} = 385 nm for **PC$_3$**). Interestingly, the solutions of these compounds undergo photo-transformation (under 254 nm UV light) with a colour change from yellow to purple, orange, and brown, respectively, for **PC$_1$–PC$_3$**, accompanied by a redshift of 120–140 nm in the absorption maxima. This transformation is rapid (within 60 seconds) and reverts to its original state by heating the solution at 35 °C for 30 minutes. In addition, **PC$_1$–PC$_3$** also exhibit variations in fluorescence, with **PC$_1$** and **PC$_2$** red-shifting by 150 nm (yellow to red emission) and **PC$_3$** undergoing complete quenching. We attribute this transformation to a photoexcited partial proton transfer, leading to a metastable hydrogen bonding state, as supported by ^{1}H NMR and DFT calculations.

Introduction

Chromic materials are smart materials that undergo a reversible change in response to heat, light, electricity, chemicals, and mechanical force. As a result, they alter the optical properties; these materials are widely used in sensors, displays, and smart coatings, among other applications.[1–8] Among the various chromic materials, photochromic systems offer significant advantages due to activation by light, which is a non-invasive, environmentally friendly, and sustainable energy source.[9] These systems exhibit reversible colour changes upon UV or visible light exposure. This phenomenon occurs due to the structural transformation between two forms, resulting from a change in the optical properties of the compounds.[10] The photochromic materials have diverse applications in optical and photonics,[11,12] display technology,[13] data storage,[14,15] biological sensing,[16] smart materials,[17,18] *etc.* Photochromism occurs in both inorganic and organic materials. Inorganic photochromic materials, such as transition metal oxides (WO_3, TiO_2, V_2O_5, Nb_2O_5, and MoO_3), have gained attention in the photochromic field due to their high thermal stability, long cycling life, and thermal/chemical resistance. However, these materials suffer from tunability (difficult to modify structure) and a complex synthetic process.[19–22] In contrast, organic photochromic materials exhibit outstanding structural flexibility and can be easily modified, making them more versatile for specific applications.[23–27] Several organic photoswitch derivatives have been reported. Among them, azobenzene, which undergoes *cis–trans* isomerisation, and diarylethene and spiropyran, which undergo ring-opening/closing upon shining light, are highly explored.[14,28–30] On the other hand, photochromic systems that undergo reversible colour changes based on changes in intramolecular hydrogen bonding interactions have found significant interest due to their high rate of conversion, precise colour tuning, and enhanced stability (Chart 1).

Ivan Ap *et al.*[31] reported the quinoline-substituted hydrazone (*E*) photoswitch in the solution state; after shining the 442 nm light, the *Z* isomer converted to an *E* isomer with a colour change from yellow to colourless, and the *Z* isomer completely reversed back to *Z* after shining the 340 nm light. Newhouse *et. al.*[32] and Castellano *et al.*[33] developed hemithioindigo- or dicyanorhodanine-pyrrole-based photoswitches, where upon shining the UV-light (405 nm), the system converts from *Z* to *E* with a considerable redshift in the absorption spectra from 503/436 nm to 567/466 nm. The *E*-isomer develops an intramolecular H-bonding pyrrole N–H with the adjacent carbonyl group. Besides, excited-state intramolecular hydrogen bonding (ESIPT) inspired photochromism has also been studied. For example, Tang *et al.*,[34] Yoon *et al.*[35] and Li *et al.*[36] developed salicylaldehyde-containing photoswitches that, upon photoexcitation, undergo enol to keto conversion, resulting in a change of colour and fluorescence. The keto form reverts to the enol form when exposed to visible light. Along similar lines, Bernard M. *et al.*,[37] reported a triaryl hydrazone-based ESIPT photoswitch. The compound under light turns the hydrazo

Department of Chemistry, IIT Dharwad, Dharwad, 580011, Karnataka, India. E-mail: rajesh@iitdh.ac.in

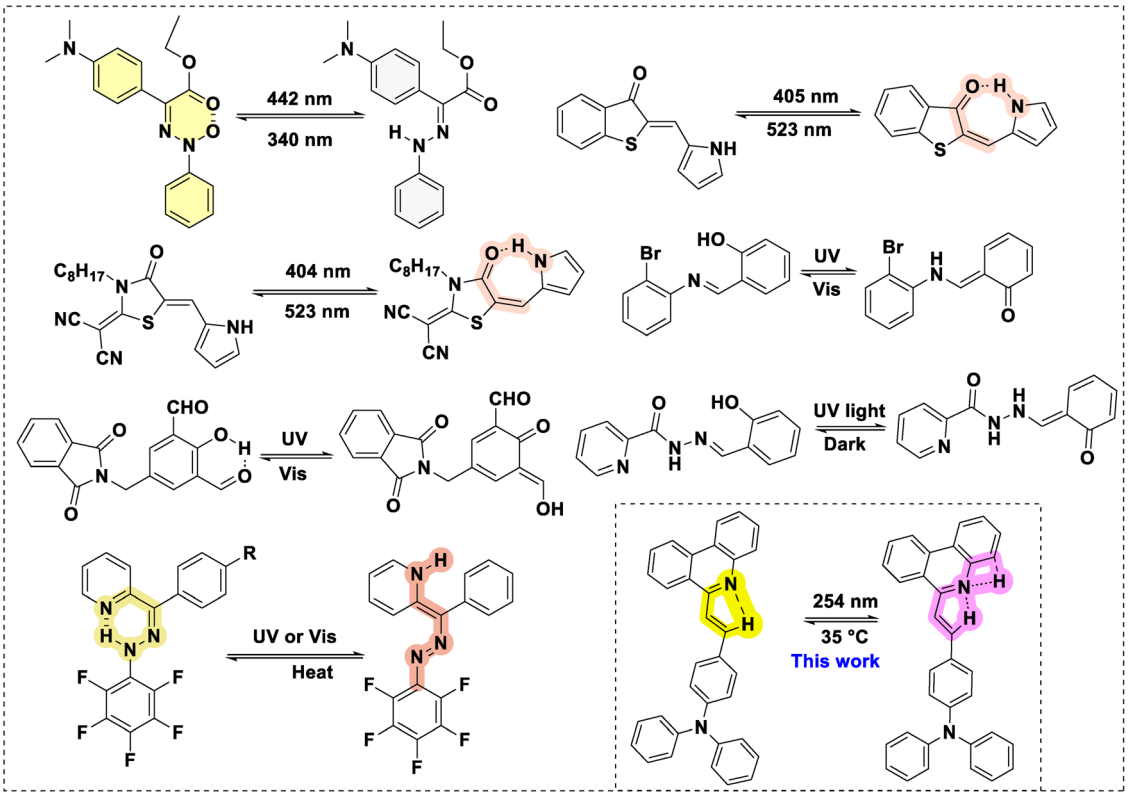

Chart 1 Reported photochromic systems based on hydrogen-bonding.

(═N–NH–) to azo (–N═N–) with an associated colour change from yellow to red. Overall, to the best of our knowledge, there are only a few examples of H-bonding-promoted photochromic systems known.

Here we report phenanthridine-based H-bonding-based photochromic systems (**PC$_1$–PC$_3$**) for the first time. The compounds (**PC$_1$–PC$_3$**) have been developed through the Knoevenagel condensation of triphenylaminyl (TPA) and pyrinyl (PY) aldehydes with an active-methyl-containing phenanthridine (**6 and 7**) in yields of 63–70%. **PC$_1$–PC$_3$** exhibit donor–acceptor interactions and, thus, absorb strongly in the visible region (λ_{abs} = 300–410 nm). **PC$_1$–PC$_3$** display photochromic behaviour upon exposure to UV light, changing their colours from yellow to purple, orange, and brown, respectively, and reverting to their original state upon heating. Similarly, the fluorescence of **PC$_1$–PC$_3$** has also been influenced by light exposure, which turns yellow to red for **PC$_1$–PC$_2$**, while it is quenched for **PC$_3$**. The photo-transformation has been attributed to photoexcited partial proton transfer leading to a metastable hydrogen bonding state upon light irradiation, as supported by ^{1}H NMR and DFT calculations.

Results and discussion

The photochromic phenanthridine systems were synthesised in several steps, as depicted in Scheme 1. The synthesis begins with the Suzuki–Miyaura coupling of 2-bromobenzene with aryl boronic acids (a and b), yielding 2-arylbenzenes (**2** and **3**). The subsequent N-acylation of the amine can be accomplished using acetyl chloride in dichloromethane to obtain compounds **4** and **5**. Furthermore, **4** and **5** were subjected to a Bischler–Napieralski cyclization using $POCl_3$ under reflux conditions, rendering the key building blocks, 2-methyl-phenanthridine derivatives (**6** and **7**). Finally, the target compounds (**PC$_1$**, **PC$_2$**, and **PC$_3$**) have been achieved by performing a Knoevenagel condensation on **6** and **7** with triphenylaminyl (TPA) and pyrenyl (PY) aldehydes in the presence of benzoic acid and benzoic anhydride. The compounds have been obtained in moderate to good yields (63–70%) and characterised with NMR and HRMS.

Crystal structure and density functional theory

The crystal structure of **PC$_1$** indicates that the entire molecular backbone adopts a planar conformation, which supports extended π-delocalisation. In addition, the imine-N is found to exert bonding interactions with the β-carbon of the vinylene (2.44 Å) and thus the substituents remain in the *trans*-conformation (Scheme 1a, b and Fig. S1 and Tables S1–S5). The compounds have also been studied by Density Functional Theory (DFT: B3LYP/6-311G(d) level of theory) to evaluate the geometry-optimised structures and electronic properties (Fig. 1). The optimized structures of **PC$_1$–PC$_3$** exhibit a planar conformation, with the torsional angle between the vinyl and phenanthridine of 0.17°, matching closely that of the crystal structure of **PC$_1$** (0.11°). The Highest Occupied Molecular

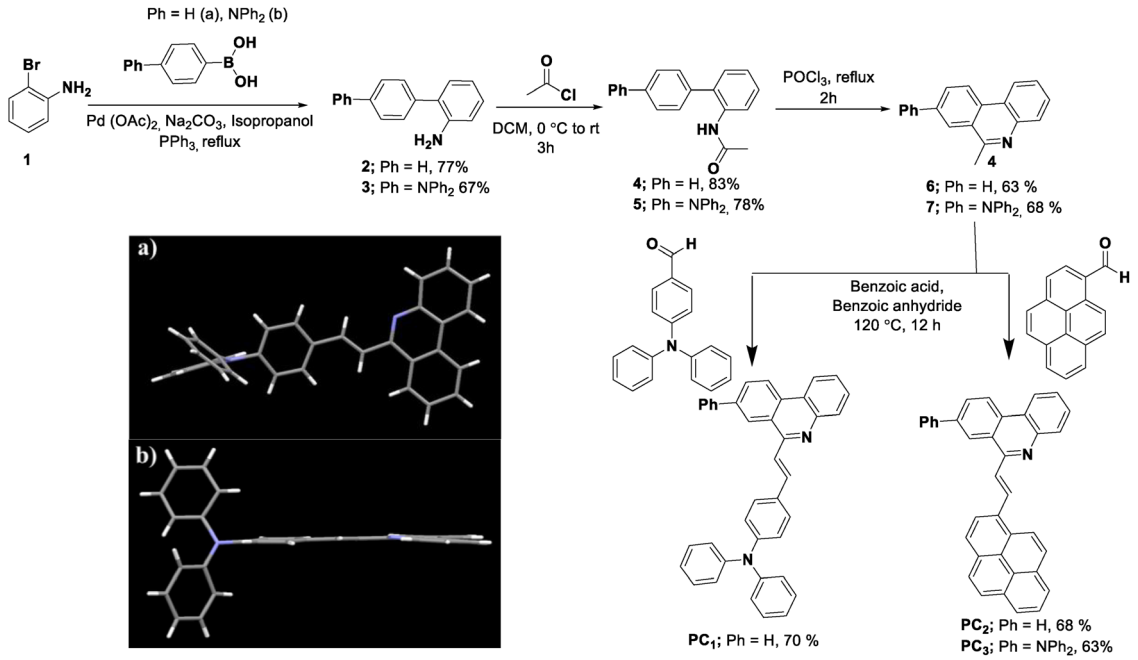

Scheme 1 Synthesis of aryl-vinylene phenanthridine-based photoswitches; crystal structure of compound $\mathbf{PC_1}$ (CCDC: 2351276): (a) top view and (b) side view.

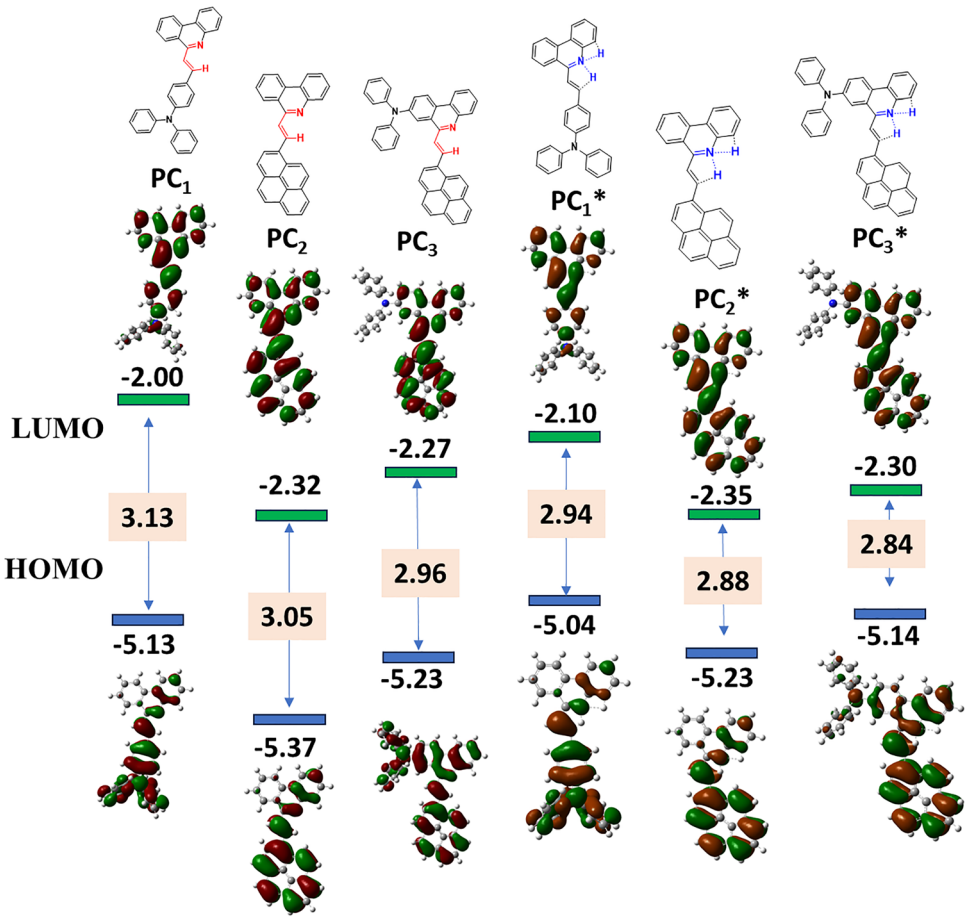

Fig. 1 DFT-optimised energy level diagram of the HOMOs and LUMOs of $\mathbf{PC_1}$–$\mathbf{PC_3}$ and their photo-transformed products $(\mathbf{PC_1^*} - \mathbf{PC_3^*})$.

Orbitals (HOMOs) of PC_1 and PC_2 are mainly localized on the aryl units due to their electron-donating nature. In contrast, the HOMO of PC_3 is delocalized across the entire molecule, due to the strong electron-donating diphenylamine unit connected to the phenanthridine core. On the other hand, the Lowest Unoccupied Molecular Orbital (LUMO) of PC_1 is mainly localised on the phenanthridine unit, whereas in PC_2 and PC_3, it is delocalized over the aryl and phenanthridine units. The HOMO and LUMO energies of PC_1, PC_2 and PC_3 have been found to be −5.13/−2.00, −5.37/−2.32 and −5.23/−2.27 eV, and the band gaps are 3.13, 3.05, and 2.96 eV, respectively. This indicates that the aryl substitution significantly affects the HOMO and LUMO energy levels: compared to PC_1, the LUMO energies of PC_2 and PC_3 are lowered by 0.3 eV and 0.2 eV, while the HOMO energy of PC_1 is higher than that of PC_2 and PC_3 by 0.2 eV and 0.1 eV, respectively. In addition, the band gap of PC_3 is found to be smaller than those of PC_1 and PC_2 by 0.04 eV and 0.1 eV, respectively, due to the strong donor–acceptor (D–A) interactions between the diphenylamine and phenanthridine units.

Optical properties

The UV-Vis absorption spectra of PC_1, PC_2, and PC_3 in $CHCl_3$ solution exhibit one or two strong π → π* transitions in the visible region (300 to 410 nm) (Fig. 2) with absorption maxima at 308 and 410 nm (ε = 16 250 and 29 390 = M^{-1} cm^{-1}) for PC_1, 364 nm (29 390 $M^{-1}{\cdot}cm^{-1}$) for PC_2, and broad band 300–500 (29 390 M^{-1} cm^{-1}) for PC_3. At the same time, a blue shift of 25–46 nm is observed for PC_2 compared to PC_1, due to strong donor–acceptor interaction, while PC_3 exhibits a broad absorption band. The broad absorption spectrum of PC_3 could be attributed to several signals resulting from (a) vibronic transitions of pyrene and (b) strong intramolecular charge transfer (ICT) transitions between triphenylamine (donor) and phenanthridine (acceptor). The ICT in PC_3 will be significantly higher due to greater π–π communication between the donor and acceptor.

Recording the absorption spectra of PC_1–PC_3 in different solvents resulted in no change in the peak positions (only a variation of 3–5 nm), indicating minimal influence of solvent polarity (Fig. S2). PC_1–PC_3 have been found to be fluorescent in the solution state. The chloroform solutions of PC_1–PC_3 display green, cyan and yellow fluorescence with emission maxima at 518 (fluorescence quantum yields, ϕ_f = 45%), 500 (ϕ_f = 15%) and 550 nm (ϕ_f = 55%), upon excitation (λ_{ex}) at 405 nm, 365 nm and 420 nm, respectively (Fig. 2b). The emission spectra in different solvents vary significantly, with a redshift of 90–100 nm in polar solvents, emphasising the strong D–A interactions (Fig. S3).

Photochemistry

PC_1–PC_3 exhibited photochromic properties upon irradiation with a 254 nm light source. All the compounds exhibit positive photochromism, displaying a bathochromic shift in their absorption bands (324 to 546 nm). Upon shining the light for 30 secs, the photo excited systems (PC_1^* – PC_3^*) displayed new absorption bands in the red region: 324, 546 nm (ε = 19110, 36160 M^{-1} cm^{-1}); 346, 512 nm (ε = 24670, 14710 M^{-1} cm^{-1}) and 345, 515 nm (ε = 37820, 14850 M^{-1} cm^{-1}), respectively (Fig. 3 and Fig. S4). When the light was irradiated at an interval of 5 seconds, the spectrum gradually changed from PC to PC* and reached a final state, characterised by two isosbestic points at 356 nm and 455 nm for PC_1, and the colour of the solution changed from yellow to purple (Fig. 3a and Fig. S4a). A similar observation was found in PC_2 and PC_3; PC_2 also shows two absorption bands at 284 and 364 nm, which disappear, and new bands at 346 and 512 nm appear, with isosbestic points at 306 and 396 nm, upon light irradiation. The colour of the solution also changes from light yellow to orange (Fig. 3b and Fig. S4b). PC_3 exhibits a broad absorption band from 300 to 500 nm, which, upon UV radiation, splits into three new bands at 278, 345, and 520 nm, accompanied by three isosbestic points at 280, 262, and 454 nm. The colour changed from yellow to brown (Fig. 3c and Fig. S4c). The significant redshift in the absorption can be attributed to the increased donor–acceptor interactions within the molecule upon photoexcitation. This could be possible if the photo-excited state promotes photoinduced partial proton transfer, leading to the formation of a phenanthridine carbocation. Such molecular transformation enhances the donor–acceptor interactions within the molecule, altering its optical properties (Fig. 3g). Photochromic kinetics studies of PC_1–PC_3 in the solution state have been conducted. The rate constant for the forward photochromic step

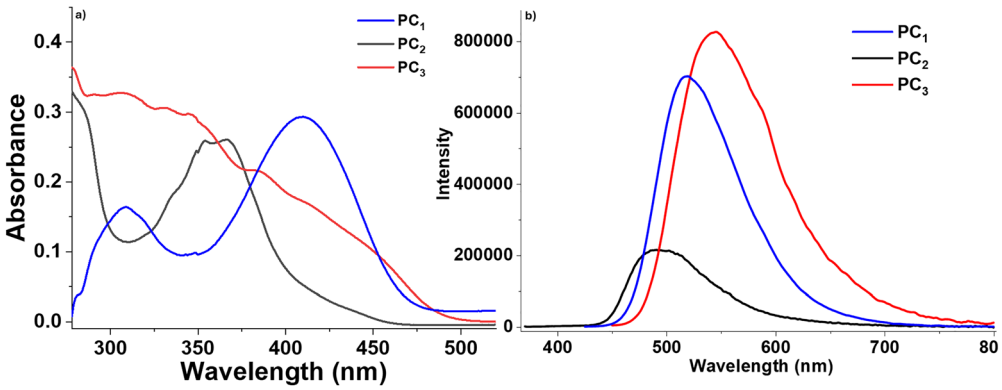

Fig. 2 (a) Absorption spectra ($CHCl_3$, 1 × 10^{-5} M) and (b) emission spectra ($CHCl_3$, 1 × 10^{-6} M) of PC_1–PC_3.

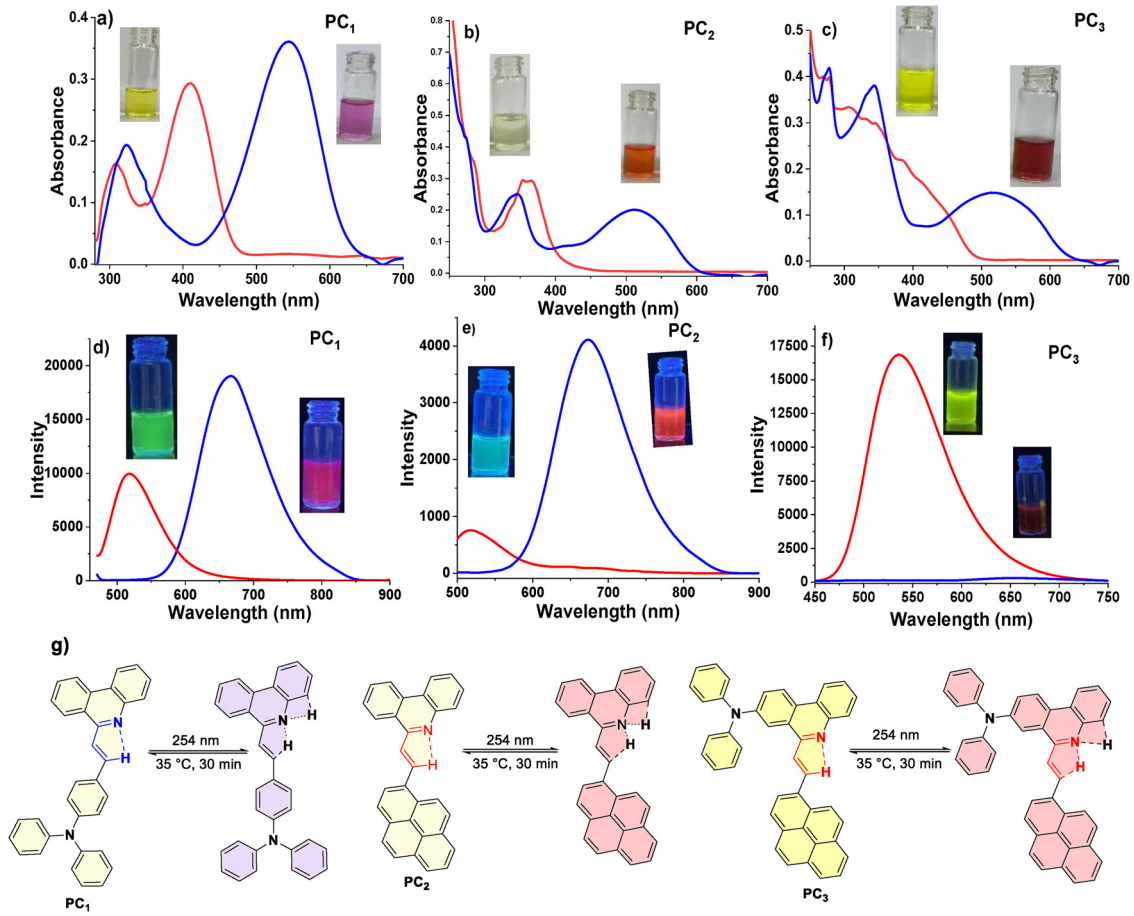

Fig. 3 Absorption spectra [(a)–(c) ($CHCl_3$, 1×10^{-5} M)]; emission spectra [(d)–(f) ($CHCl_3$, 1×10^{-6} M)] of **PC_1–PC_3** (before irradiation (red line) and after irradiation at 254 nm (blue line); (g) schematic representation of photoexcited partial proton transfer forming a metastable hydrogen-bonded state.

in **PC_1–PC_3** was found in the range of $3 \times 10^{-2} - 12 \times 10^{-2}$ sec^{-1}. The photochromic change was found to be faster in the case of **PC_3**, followed by **PC_2** and **PC_1**, which is reflected in their rate constants. The quantum efficiency of the **PC_1–PC_3** colouring process was found to be 16–27%. On the other hand, the rate constants for the thermal reversibility of **PC_1–PC_3** are in the range of 10×10^{-2} to 76×10^{-2} min^{-1} with the order of **PC_2** > **PC_3** > **PC_1** (Fig. S37 and S38 and Table S6).

Interestingly, we have also found that the fluorescence of the photo-transformed products of **PC_1–PC_3** changes significantly upon light irradiation (Fig. 3d–f and Fig. S5). Upon light irradiation, the fluorescence signal of **PC_1** shifted from 518 nm to 665 nm, exhibiting a redshift of 147 nm, accompanied by an increase in emission intensity. Moreover, the fluorescence colour has changed from green to orange-red (Fig. 3d and Fig. S5a). The same observation was found for **PC_2**, which showed a redshift of 154 nm in the emission maximum from 520 nm to 672 nm (Fig. 3e and Fig. S5b). On the other hand, the fluorescence of **PC_3** (536 nm) was completely quenched after applying the UV light (Fig. 3f and Fig. S5c). The fluorescence quantum yields of light-irradiated samples **PC_1^*** and **PC_2^*** were increased to $\phi_f = 58\%$ and 65%, respectively. We have also tested the photo-transformation of **PC_1** under sunlight, which showed similar spectral and colour changes as the UV lamp; however, the complete conversion takes about 2 h (Fig. 5a). The reversible process of the photoexcited compounds can be triggered by heating the samples at 35 °C for 30 min (Fig. 4). Moreover, the system exhibits excellent stability with little degradation for **PC_1** in absorbance over five cycles of photoexcitation and heating (Fig. 5b). The solid-state photochromic behaviour was also tested by dispersing **PC_1** in a polymer matrix. The blend of **PC_1** and PMMA (polymethyl methacrylate) exhibits photochromism when illuminated for 5 minutes, changing the colour (colourless to pink) and fluorescence (cyan to red) of the coated film. The process is also found to be reversible, as evidenced by heating the film at 50 °C for 10 minutes (Fig. 6a).

The performance of **PC_1–PC_3** has been compared to the reported ESIPT systems (Table S6). **PC_1–PC_3** are comparable to the reported systems in terms of stability, switching time, and reversibility. Moreover, **PC_1–PC_3** possess several unique features, such as (a) tunability of the photochromic colours by changing the substituents; (b) tunable photofluorochromic behaviour, such as turn-on fluorescence along with emissive colour modulation for **PC_1** and **PC_2** and turn-off fluorescence for **PC_3**; and (c) large red shift of 154 nm in the emission signal,

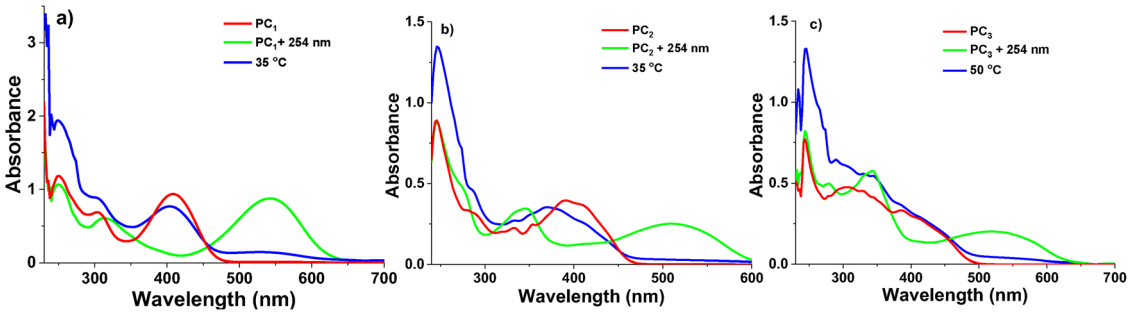

Fig. 4 Reversibility analysis of (a) **PC_1**, (b) **PC_2**, and (c) **PC_3** after heating at 35 °C for 30 minutes.

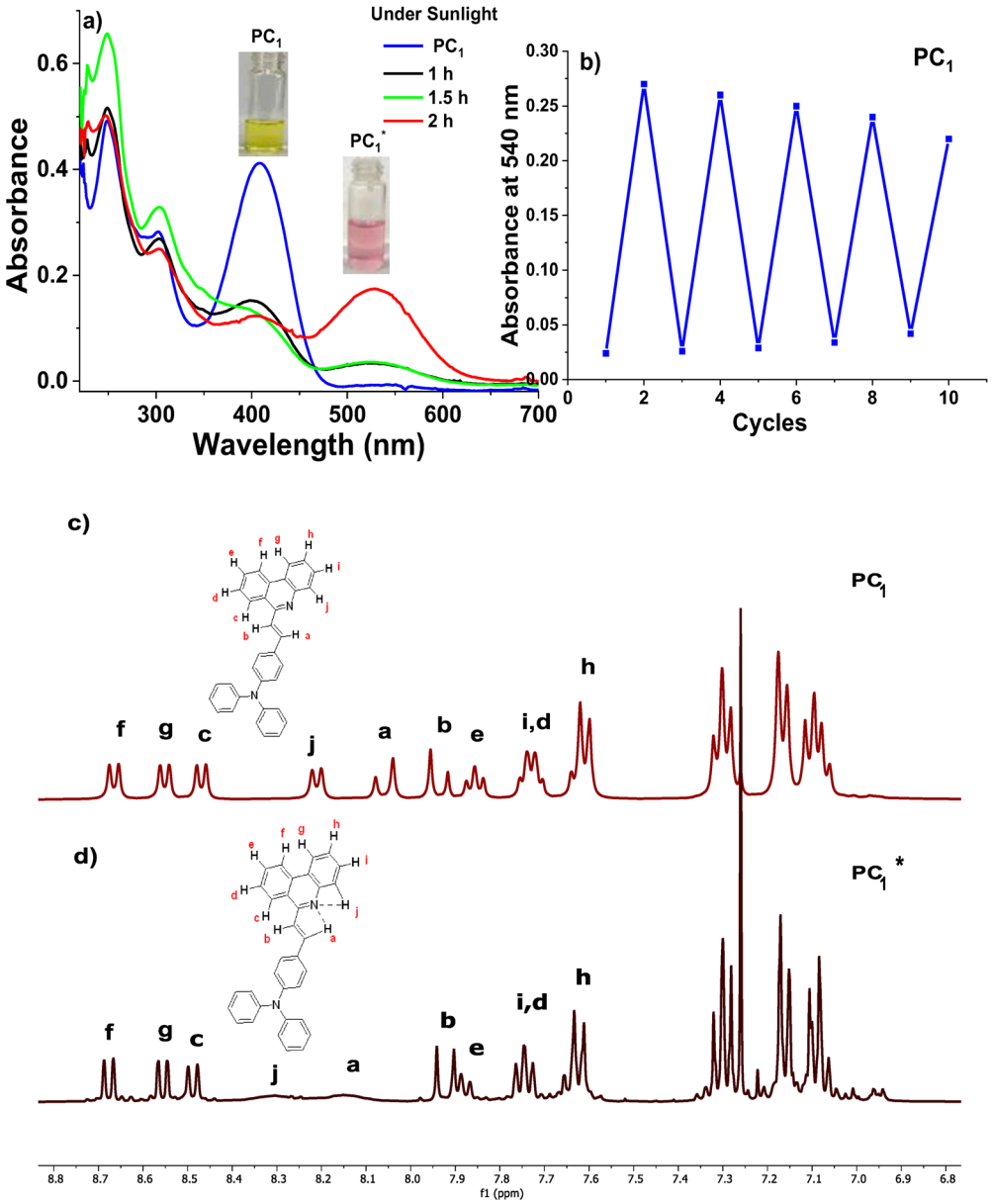

Fig. 5 (a) Absorption spectra of compound **PC_1** under sunlight, (b) photo-transformation cycles of **PC_1** (1×10^{-5} M) in $CHCl_3$; the absorbance change at λ_{max} = 540 nm was monitored under irradiation at 254 nm and during heating at 35 °C; ^{1}H NMR spectra (400 MHz, $CDCl_3$) of compound **PC_1** before (c) and after (d) exposure to UV light.

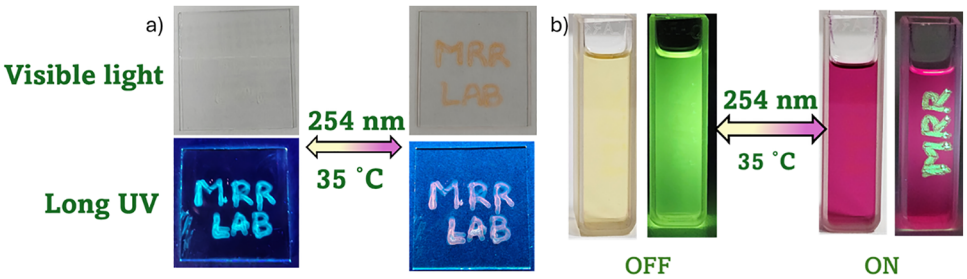

Fig. 6 (a) The usage of the PC_1 and PMMA blend in the application of anticounterfeiting and (b) the usage of PC_1 solution in chloroform and showing its application in signboards.

which helps to avoid the overlap of colours, and obtain pure colours.

Time-resolved fluorescence decay measurements of PC_1–PC_3 were carried out in chloroform (Fig. S6). Before irradiation, the fluorescence decay profiles of PC_1 and PC_3 were best fitted with a single exponential function, yielding lifetimes of τ = 1.18 ns (100%) for PC_1 and τ = 6.35 ns (100%) for PC_3. In contrast, PC_2 exhibited a biexponential decay with components τ_1 = 0.30 ns (97%) and τ_2 = 3.0 ns (3%). Upon photoirradiation, both PC_1 and PC_2 showed biexponential decay behaviour. The photo-irradiated PC_1 exhibited lifetimes of τ_1 = 1.2 ns (95.45%) and τ_2 = 5.0 ns (4.55%), while photo-irradiated PC_2 showed τ_1 = 1.5 ns (92.04%) and τ_2 = 5.0 ns (7.96%). The longer lifetimes of PC_1^* and PC_2^* indicate that these species possess stable charge–transfer states.

To understand the mechanism of the photo-transformation, PC_1 has been studied using ^{1}H NMR spectroscopy before and after photo-irradiation (Fig. 5c and d). Interestingly, the ^{1}H NMR spectra of PC_1, before and after light irradiation, match closely (with a variation of 0.01–0.02 ppm) with each other except for the two protons corresponding to the β-proton of vinylene and the *j*-proton of phenanthridine. These proton signals have been broadened and experienced a downfield shift from 8.06 ppm to 8.15 ppm for the β-proton of the vinylene and from 8.20 ppm to 8.30 ppm for the *j*-proton of the phenanthridine. The ^{1}H NMR studies suggest that PC_1, upon light irradiation, (1) undergoes minimal structural changes, indicating that there is no isomerisation; (2) the β-proton of vinylene and *j*-proton of phenanthridine possess a labile nature; (3) sharp signals indicate that there is no radical formation.

Furthermore, we have also conducted FT-IR and cyclic voltametric analysis on PC_1 and PC_1^*. In FT-IR, the stretching frequency of C=N in PC_1 changes from 1589 cm^{-1} to 1575 cm^{-1} for PC_1^*. On the other hand, in cyclic voltammetry, the oxidation potential of PC_1 shifts anodically from 1.06 V (*vs.* Ag/AgCl) to 1.23 V (*vs.* Ag/AgCl) for PC_1^*. FT-IR reveals that C=N is more polarised towards a higher single bond character, while cyclic voltammetry shows a reduction in the electron density on the nitrogen atom of the phenanthridine unit.

Based on the results obtained from the above experiments, we hypothesise that a light-induced hydrogen bonding interaction might exist between the β-proton of vinylene and the *j*-proton of phenanthridine with the phenanthridine nitrogen, leading to partial proton transfer to the phenanthridine moiety (Fig. 5c, d and Fig. 3g). Further studies are necessary to prove this hypothesis.

To validate our hypothesis, DFT-optimisation has been carried out on $PC_1^* - PC_3^*$. The photoexcited systems exhibit no structural changes with respect to PC_1–PC_3, which supports the minimal changes observed in the ^{1}H NMR. The HOMO energy of $PC_1^* - PC_3^*$ compared to their pristine samples has been found to increase by 0.09–0.14 eV, while the LUMO energy decreases by 0.03–0.10 eV, resulting in a significant reduction in the band gaps (0.12–0.20 eV). $PC_1^* - PC_3^*$, compared to PC_1–PC_3, have also been found to be less stable by 56.2, 55.2 and 55.3 Kcal/mol than the PC_1^*, PC_2^* and PC_3^*, respectively. These changes indicate the formation of a metastable state involving partial proton transfer upon exposure to light. This process enhances donor–acceptor (D–A) interactions, resulting in band gap reductions of 0.20 eV for PC_1, 0.17 eV for PC_2 and 0.12 eV for PC_3 (Fig. 1). The absorption spectra of PC_1–PC_3 and their photoexcited systems ($PC_1^* - PC_3^*$) optimised using TD-DFT have also supported the experimental data (Fig. S7).

The solid-state photochromic behaviour of PC_1 can be used as an anticounterfeiting ink. A dichloromethane solution of a blend of PMMA and PC_1 was used to write the MRR lab word on a glass slide, which remained invisible after writing. Upon exposure to light, the PC_1 changed its colour to pink, and the word became visible. The process was found to be reversible upon heating the glass slide at 35 °C (Fig. 6a). Under long UV, the fluorescence of the word changed from cyan to red, which can be used for signboards. A similar behaviour was also observed in the solution (Fig. 6b).

Conclusion

In conclusion, three photochromic systems based on phenanthridine have been developed by condensing active methylene-substituted phenanthridine units (**6** and **7**) with several aromatic aldehydes [triphenylaminyl (TPA), and pyrenyl (PY)] in the presence of benzoic acid and benzoic anhydride. The compounds have been thoroughly characterised using ^{1}H NMR, HRMS, and single-crystal XRD (for PC_1). PC_1–PC_3 have been studied to exhibit photochromic behaviour under UV light (254 nm). The photo-transformation changes the absorption maxima of PC_1–PC_3 from 330–350 nm to 550–600 nm and

the colour from yellow to purple/orange/brown. Moreover, **PC_1–PC_3** also exhibit a fluorescence change, turning on red emission (λ_{em} = 665–675 nm). The photo-transformation has been characterised by UV-Vis absorption, fluorescence and ^{1}H NMR spectroscopy. The studies indicated that the compounds undergo a photoexcited partial proton transfer, leading to a metastable hydrogen bonding state.

Conflicts of interest

There are no conflicts to declare.

Data availability

The supporting data for this article have been included in the supplementary information (SI). Supplementary information contains synthetic experimental procedures, NMR spectral data, cyclic voltammograms, solvatochromic studies of UV-Vis absorption and fluorescence emission, crystal data, FT-IR, life time data. See DOI: https://doi.org/10.1039/d5tc02868j.

CCDC 2351276 contains the supplementary crystallographic data for this paper.[38]

Acknowledgements

Rajeswara Rao thanks SERB, India, and IIT Dharwad for partially supporting this research through a Core Research Grant (CRG/2023/002129). The authors are grateful to the Sophisticated Central Instrumentation Facility (SCIF), IIT Dharwad, and all its staff members for letting them use the facilities and assisting them with the material characterisation studies.

References

1 O. S. Wenger, *Chem. Rev.*, 2013, **113**, 3686–3733.
2 H. Zhang and X. Wu, *Adv. Sci.*, 2016, **3**, 1500224.
3 C. Gu, A.-B. Jia, Y.-M. Zhang and S. X.-A. Zhang, *Chem. Rev.*, 2022, **122**, 14679–14721.
4 C. Sun, M.-S. Wang, P.-X. Li and G.-C. Guo, *Angew. Chem., Int. Ed.*, 2017, **56**, 554–558.
5 P. Xue, J. Ding, P. Wang and R. Lu, *J. Mater. Chem. C*, 2016, **4**, 6688–6706.
6 Y. Mi, H.-B. Cheng, H. Chu, J. Zhao, M. Yu, Z. Gu, Y. Zhao and L. Li, *Chem. Sci.*, 2019, **10**, 10231–10239.
7 H. Beyrami, M. Golshan, A. Zardehi-Tabriz and M. Salami-Kalajahi, *Adv. Mater. Technol.*, 2025, e00574.
8 A. Priimagi, C. J. Barrett and A. Shishido, *J. Mater. Chem. C*, 2014, **2**, 7155–7162.
9 J. Zhang and H. Tian, *Adv. Opt. Mater.*, 2018, **6**, 1701278.
10 M. Morimoto and M. Irie, *Chem. Commun.*, 2005, 3895–3905.
11 Y. Wakayama, R. Hayakawa, K. Higashiguchi and K. Matsuda, *J. Mater. Chem. C*, 2020, **8**, 10956–10974.
12 A. Szukalski, A. Korbut, K. Zieniewicz and S. Zielińska, *J. Phys. Chem. B*, 2021, **125**, 13565–13574.
13 P. Li, Y. Wang, X. He, Y. Cui, J. Ouyang, J. Ouyang, Z. He, J. Hu, X. Liu, H. Wei, Y. Wang, X. Lu, Q. Ji, X. Cai, L. Liu, C. Hou, N. Zhou, S. Pan, X. Wang, H. Zhou, C.-W. Qiu, Y.-Q. Lu and G. Tao, *Light: Sci. Appl.*, 2024, **13**, 48.
14 M. Irie, T. Fukaminato, K. Matsuda and S. Kobatake, *Chem. Rev.*, 2014, **114**, 12174–12277.
15 S. Kawata and Y. Kawata, *Chem. Rev.*, 2000, **100**, 1777–1788.
16 J. Zhang, J. Wang and H. Tian, *Mater. Horiz.*, 2014, **1**, 169–184.
17 H. Torres-Pierna, D. Ruiz-Molina and C. Roscini, *Mater. Horiz.*, 2020, **7**, 2749–2759.
18 L. Wang and Q. Li, *Chem. Soc. Rev.*, 2018, **47**, 1044–1097.
19 J. Du, Z. Yang, H. Lin and D. Poelman, *Responsive Mater.*, 2024, **2**, e20240004.
20 Y. Badour, V. Jubera, I. Andron, C. Frayret and M. Gaudon, *Opt. Mater.*, 2021, **12**, 100110.
21 A. B. A. Kayani, S. Kuriakose, M. Monshipouri, F. A. Khalid, S. Walia, S. Sriram and M. Bhaskaran, *Small*, 2021, **17**, 2100621.
22 Y. Chen, T. Gong, Q. Han, J. Liu, L. Chen and J. Zhao, *ACS Appl. Mater. Interfaces*, 2025, **17**, 1682–1693.
23 Y. Ru, Z. Shi, J. Zhang, J. Wang, B. Chen, R. Huang, G. Liu and T. Yu, *Mater. Chem. Front.*, 2021, **5**, 7737–7758.
24 J. Wang, Y. Yang, L. Zhang and Z. Li, *Adv. Mater.*, 2025, **37**, 2503074.
25 V. A. Barachevsky, *J. Photochem. Photobiol., A*, 2018, **354**, 61–69.
26 W. Wang, Y. Cheng and X. Xie, *Chem. Commun.*, 2025, **61**, 8327–8338.
27 Y. Zhuang, X. Ren, X. Che, S. Liu, W. Huang and Q. Zhao, *Adv. Photonics*, 2020, **3**, 014001.
28 H. M. D. Bandara and S. C. Burdette, *Chem. Soc. Rev.*, 2012, **41**, 1809–1825.
29 M. Irie, *Chem. Rev.*, 2000, **100**, 1685–1716.
30 R. Klajn, *Chem. Soc. Rev.*, 2013, **43**, 148–184.
31 B. Shao, M. Baroncini, H. Qian, L. Bussotti, M. Di Donato, A. Credi and I. Aprahamian, *J. Am. Chem. Soc.*, 2018, **140**, 12323–12327.
32 J. E. Zweig and T. R. Newhouse, *J. Am. Chem. Soc.*, 2017, **139**, 10956–10959.
33 P. Das, N. J. Grinalds, I. Ghiviriga, K. A. Abboud, Ł. Dobrzycki, J. Xue and R. K. Castellano, *J. Am. Chem. Soc.*, 2024, **146**, 11932–11943.
34 X.-M. Cai, Y. Lin, Y. Li, X. Chen, Z. Wang, X. Zhao, S. Huang, Z. Zhao and B. Z. Tang, *Nat. Commun.*, 2021, **12**, 1773.
35 Y. Chen, Y. R. Lee, W. Wang, Y. Fang, S. Lu, J. Han, X. Chen, M. H. Kim and J. Yoon, *Angew. Chem., Int. Ed.*, 2023, **62**, e202301765.
36 Y. Li, H. Li, W. Jin, X. Xu, H. Liu, Y. Ding, G. Wang, T. Zhang, Q. Peng, J. He, Q. Hu, L. Pan and K. Li, *Dyes Pigm.*, 2022, **202**, 110295.
37 B. Mravec, Š. Budzák, M. Medved', L. F. Pašteka, P. Lazar, E. Procházková, A. Růžička, J. Kožíšek, K. Vegso, M. Bodik, P. Šiffalovič, P. Švec, J. Filo and M. Cigáň, *J. Am. Chem. Soc.*, 2025, **147**, 2421–2431.
38 CCDC 2351276: Experimental Crystal Structure Determination, 2025, DOI: 10.5517/ccdc.csd.cc2jxpms.

